ADVANCED MATERIALS
www.advmat.de

Zwitterionic Dendrimersomes: A Closer Xenobiotic Mimic of Cell Membranes

*Anton Joseph, Anna M. Wagner, Manuela Garay-Sarmiento, Mina Aleksanyan, Tamás Haraszti, Dominik Söder, Vasil N. Georgiev, Rumiana Dimova, Virgil Percec, and Cesar Rodriguez-Emmenegger**

Building functional mimics of cell membranes is an important task toward the development of synthetic cells. So far, lipid and amphiphilic block copolymers are the most widely used amphiphiles with the bilayers by the former lacking stability while membranes by the latter are typically characterized by very slow dynamics. Herein, a new type of Janus dendrimer containing a zwitterionic phosphocholine hydrophilic headgroup (JD^{PC}) and a 3,5-substituted dihydrobenzoate-based hydrophobic dendron is introduced. JD^{PC} self-assembles in water into zwitterionic dendrimersomes (z-DSs) that faithfully recapitulate the cell membrane in thickness, flexibility, and fluidity, while being resilient to harsh conditions and displaying faster pore closing dynamics in the event of membrane rupture. This enables the fabrication of hybrid DSs with components of natural membranes, including pore-forming peptides, structure-directing lipids, and glycans to create raft-like domains or onion vesicles. Moreover, z-DSs can be used to create active synthetic cells with life-like features that mimic vesicle fusion and motility as well as environmental sensing. Despite their fully synthetic nature, z-DSs are minimal cell mimics that can integrate and interact with living matter with the programmability to imitate life-like features and beyond.

1. Introduction

The goal of bottom-up synthetic biology is to design and build a fully synthetic protocell. This endeavor promises to produce minimal systems to probe biological questions, shed light on the origin of life and enable new biotechnologies beyond the limits of nature. Without the complexity and redundancies that are present in natural cells, these synthetic systems offer a more predictable and efficient mean.[1]

Arguably, one of the most important components of a cell is its membrane. In nature, the main structural components of cell membranes are phospholipids. They consist of a zwitterionic phosphocholine (PC) head group and a variety of saturated or partially unsaturated carbon chains as tails which are connected to a glycerol core. The phospholipids act as a matrix into which a substantial number of other types of lipids, cholesterol, proteins, and carbohydrates are embedded.[2]

A. Joseph, A. M. Wagner, M. Garay-Sarmiento, T. Haraszti, D. Söder, C. Rodriguez-Emmenegger
DWI – Leibniz Institute for Interactive Materials
Forckenbeckstraße 50, 52074 Aachen, Germany
E-mail: rodriguez@dwi.rwth-aachen.de

A. Joseph, A. M. Wagner, T. Haraszti, D. Söder
Institute of Technical and Macromolecular Chemistry
RWTH Aachen University
Worringerweg 2, 52074 Aachen, Germany

M. Garay-Sarmiento
Chair of Biotechnology
RWTH Aachen University
Worringerweg 3, 52074 Aachen, Germany

The ORCID identification number(s) for the author(s) of this article can be found under https://doi.org/10.1002/adma.202206288.

DOI: 10.1002/adma.202206288

M. Aleksanyan
Institute for Chemistry and Biochemistry
Freie Universität Berlin
Takustraße 3, 14195 Berlin, Germany

M. Aleksanyan, V. N. Georgiev, R. Dimova
Max Planck Institute of Colloids and Interfaces
Science Park Golm
14476 Potsdam, Germany

V. Percec
Roy & Diana Vagelos Laboratories
Department of Chemistry
University of Pennsylvania
Philadelphia, PA 19104323, USA

C. Rodriguez-Emmenegger
Bioinspired Interactive Materials and Protocellular Systems
Institute for Bioengineering of Catalonia (IBEC)
The Barcelona Institute of Science and Technology (BIST)
Carrer de Baldiri Reixac 10–12, 08028 Barcelona, Spain
E-mail: crodriguez@ibecbarcelona.eu

C. Rodriguez-Emmenegger
Institució Catalana de Recerca i Estudis Avançats (ICREA)
Passeig Lluís Companys 23, 08028 Barcelona, Spain

The synergistic behavior of these components provides sites for reactions at the membrane surface and endows the cell with its numerous functions, such as sensing the environment, motion, or establishment of chemical potential differences for the maintenance of the out-of-equilibrium system that is life.[3]

Such advanced functions may be in reach by integrating natural receptors and functional molecules into synthetic biomembranes which faithfully mimic their native environment. First, their thickness must match one of natural membranes (4–6 nm) to allow for seamless integration of natural functional building blocks into the membrane.[4] These embedded functionalities must be able to rapidly diffuse and organize laterally inside the membrane to give rise to a multitude of multivalent interactions.[2a,5] This demands diffusion coefficients in the same order as in natural membranes (≈1 $\mu m^2 s^{-1}$). On top of that, complex functions such as endo/exocytosis, division, extension of appendages demand membranes with extremely high flexibility and stability. Natural membranes achieve these seemingly antagonistic properties by combining phospholipid bilayers with bending rigidities of just a few tens of the thermal energy with structural components that enhance the molecular cohesion and overall stability.[6]

Vesicles assembled from (phospho)lipids, called liposomes, are the system of choice for synthetic biologists under the premise that these molecules are the majoritarian components of cell membranes. Indeed, they provide faithful mimicry of most properties except for stability. In single-component liposomes, the lack of certain molecules that enhance cohesion between the lipids significantly alters their physical properties and stability compared to natural cells. Moreover, biologically relevant lipids also lack chemical stability as their double bonds are prone to oxidation and their ester bonds prone to hydrolysis.[7] Without constant repair and replenishment as in cells, these degradation processes result in new molecules with variable physical properties and biological activity which hampers the liposome's overall properties, even at low oxidation levels.[8] Microscopically, this translates into worsening of the stability, aggregation, fusion, and leakage of encapsulated material.[7] These features complicate storage, handling and limit long-term observation of liposomes, especially under irradiation conditions during microscopy.

Polymersomes assembled from amphiphilic block copolymers represent a synthetic alternative to lipids. Their higher molecular weight and entanglement of the hydrophobic blocks drastically improve the stability of their membranes.[9] Moreover, modern controlled polymerizations give access to macromolecules with precise dispersity of each block and offer a vast synthetic space for macromolecular design to control the surface topology and reactivity of the polymersome.[10] However, the higher molecular weight inevitably leads to thicker, less flexible membranes with reduced or almost frozen dynamics.[9,11] This hampers the integration of natural building blocks such as lipids, peptides, or transmembrane proteins and affects all functions requiring membrane remodeling.[12]

Most of these caveats have been alleviated with the introduction of graft copolymers. Hydrophobic, flexible poly(dimethylsiloxane) (PDMS) backbones form the hydrophobic domains of the membrane from where poly(ethylene oxide) (PEO) side chains are sparingly grafted to generate the hydrophilic periphery. Recent work has demonstrated the insertion of lipids, transmembrane proteins that are part of the respiratory cascade and of the SNARE system.[13] However, the complete mixing with lipids and PDMS-*g*-PEO was only observed for a limited range of compositions, and thus, resulted in phase separation and fission.[13c,14] These systems have been surpassed by ionic combisomes, biomimetic vesicles assembled from amphiphilic comb-polymers which demonstrated excellent mimicry of most biophysical properties and the ability to hijack complex cell membrane features.[15] However, the most advanced vesicle system is based on the self-assembly of amphiphilic Janus dendrimers (JDs) into dendrimersomes which provide a fully synthetic surrogate to lipids and glycolipids.[16] We have previously demonstrated that they can fully or partially mix with lipids, incorporate membrane proteins, carry nucleic acids, and form hybrids with natural cells to incorporate their periphery.[16a,17] Moreover, they have served as a platform to unravel how the complex 2D organization of glycans controls their reactivity and can be programmed to perform complex shape transformations akin to living cells.[18] However, the dendritic design of most JDs relied on oligo(ethylene glycol) or polyol groups as hydrophilic moieties. Such groups do not represent the periphery that natural cell membranes present to the outside and may alter the interactions of cells or natural proteins with the membrane.

In this work, we overcome this limitation by introducing a new type of zwitterionic JD that assembles into vesicles that combine the augmented properties of dendrimersomes with the PC periphery natively displayed in cells. The zwitterionic JD (JD^{PC}) was built by appending a PC hydrophilic head group to a 3,5-didodecyl benzoate hydrophobic dendron. The latter dendron provides the appropriate balance in cohesive interactions to drive the assembly into membranes that closely mimic the thickness, lateral mobility, and flexibility of liposomes. Conversely, their molecular design addresses the weak points of phospholipids resulting in an enzymatic, thermal, and mechanical stability beyond their natural counterparts. Moreover, the zwitterionic periphery of JD^{PC} provides stability in complex biological media such as blood plasma and compatibility with various cell lines. We show that the excellent level of biomimicry of JD^{PC} enables the seamless integration of components of natural membranes, such as pore forming peptides, phospho-, and glycolipids as well as, structure-directing lipids to generate raft-like domains. Furthermore, the high flexibility of zwitterionic dendrimersomes (z-DSs) membranes allows to readily fuse them with liposomes which constitutes a route toward building hybrids. Finally, sensing and motility are enabled by functionalizing the z-DSs with specific enzymes. This report demonstrates the suitability of the z-DSs to serve as a platform to build active synthetic cells that imitate life and beyond.

2. Results and Discussion

2.1. Biomimetic z-DSs

We designed and synthesized a PC-based JD (JD^{PC}) based on three considerations in our molecular design. First, the JD should structurally resemble lipids to ensure similar physical

behavior of the respective membrane. Initial reports of JDs were based on twin-twin structures, where two hydrophobic and two hydrophilic dendrons were connected to a core on opposite sites. However, we chose a single-single JD design bearing two hydrophobic chains since subsequent reports showed that such synthetically less demanding amphiphiles can also form stable and flexible DSs.[19]

Second, the hydrophobic dendron should provide additional mechanical stability to the membrane compared to lipids. We selected a dihydrobenzoate-based hydrophobic dendron since we hypothesize that π–π interactions between the aromatic rings would provide an additional cohesive force and the concomitant improved stability. We incorporated a 3,5-substitution pattern, because such DSs displayed two to six times higher energies at break compared to similar 3,4 or 3,4,5 substituted derivatives in previous micropipette aspiration experiments.[16a] The increased stability is a consequence of the more efficient interdigitation of alkyl chains in 3,5 substituted dendrons while maintaining a biomimetic thickness.[20]

Third, we chose a chain length of 12 carbon units mainly to avoid crystallization of the alkyl chains at room temperature in order to achieve flexible DSs and to yield membranes with biomimetic thickness.

We synthesized JD^{PC} according to **Figure 1**a. We introduced the hydrophobic tails in a Williamson ether synthesis using methyl 3,5-dihydrobenzoate (**1a**) and didodecylbromide.

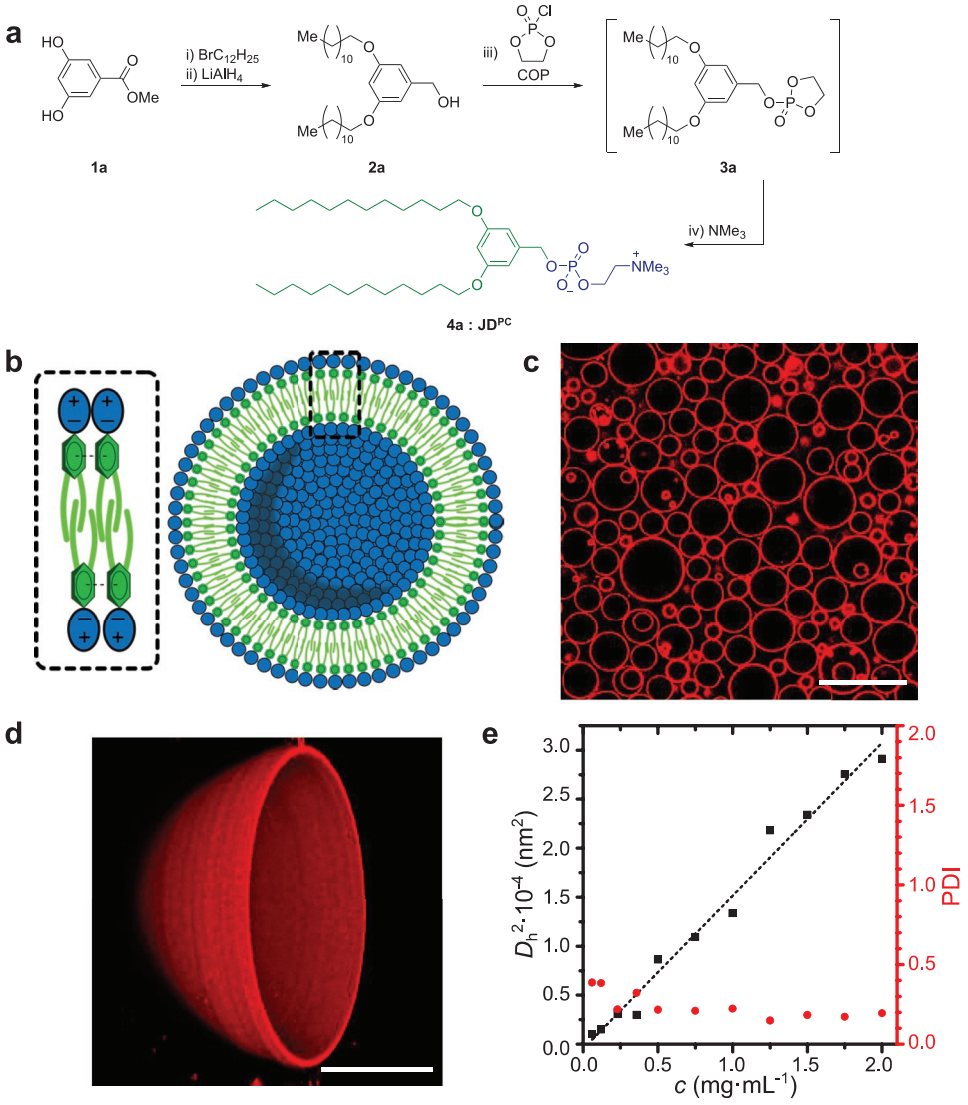

Figure 1. Self-assembly of JD^{PC} into biomimetic dendrimersomes z-DSs. a) Synthetic route toward JD^{PC}. b) Scheme of JD^{PC} highlighting the additional cohesive π–π interactions between the aromatic rings and interdigitation of the hydrophobic dendrons that drove the assembly into z-DS with improved stability. c) Giant unilamellar z-DSs assembled by electroformation method of JD^{PC} in 200×10^{-3} M sucrose. The z-DSs were labeled with 0.5 mol% Nile red. Scale bar: 50 µm. d) 3D reconstruction of 100 confocal scans showing a bisected z-DS labeled with Nile red (0.5 mol%). Scale bar: 10 µm. e) D_h of z-DS prepared at different concentrations c by injection method and determined by DLS. The D_h^2 scales linearly with the concentration and results in narrowly disperse vesicles. The polydispersity index (PDI), which measures the breadth of the distribution, was below 0.22 for all systems formed with concentrations higher than 0.4 mg mL^{-1} (red axis).

Subsequent reduction by $LiAlH_4$ afforded the respective benzylic alcohol **2a**. Following a phosphorylation, amination approach, we first utilized 2-chloro-2-oxo-1,3,2-dioxaphospholane (COP) to generate **3a**. The intermediate **3a** was used in an endocyclic ring-opening reaction by NMe_3 to yield the desired JD^{PC} (**4a**). We also observed the formation of a cationic product (JD^{cat}) which was likely formed by an exocyclic nucleophilic substitution of the cyclic phosphate by NMe_3 (Figure S5, Supporting Information). JD^{cat} was removed by flash column chromatography and the desired JD^{PC} was isolated as a colorless waxy solid in 10% yield with respect to **1**. Thermal analysis by differential scanning calorimetry of an annealed JD^{PC} sample revealed a single transition at $T_m = -14.3$ °C, well below room temperature (Figure S19, Supporting Information). This is a necessary requirement to form fluid and flexible membranes at room temperature.

We assembled JD^{PC} into z-DSs in various aqueous media using three different methods commonly employed for liposome and polymersome formation.[17b,21] We formed giant unilamellar z-DSs by thin-film hydration and electroformation. Both methods involve deposition of a thin film onto a substrate from a good solvent, followed by swelling and detachment of the bilayers in an aqueous medium. During electroformation the process is assisted by electrodewetting using a cyclic voltage. Both techniques produced mainly spherical unilamellar vesicles with a diameter of 15–45 µm for the electroformation and 2–30 µm for the thin film hydration method determined by using confocal laser scanning microscopy (CLSM) images (Figure 1c,d and Figure S20, Supporting Information for distribution of sizes). An improved vesicle yield was achieved when the assembly was carried out by electroformation in a sucrose solution. Moreover, less oligovesicular assemblies were observed for electroformation (Figure 1c). However, we found that the vesicle yields during electroformation are generally decreased when only water (no sugars, no salts) is used as a hydration medium. To study effects of vesicle size and investigate the behavior of a larger population of vesicles during our experiments, we further prepared small unilamellar DSs by the injection method. This method afforded vesicles with diameters of 40–170 nm by simply injecting an ethanolic solution of JD^{PC} into water or buffer and vortexing the resulting dispersion. Their hydrodynamic diameter (D_h) could be controlled by the concentration of JD^{PC} ($c_{JD^{PC}}$) in the resulting suspension. We found that the D_h scales with $D_h \approx c_{JD^{PC}}^{1/2}$ as previously observed for other JDs (Figure 1e) while the polydispersity index (PDI) of their size remained low with PDI < 0.22 for concentrations of at least 0.4 mg mL^{-1}.[19,20]

2.2. Biomimicry of z-DSs

Arguably, thickness, flexibility, and the ability to laterally organize components are the key physical properties that define the level of biomimicry of synthetic biomembranes. Giant and small unilamellar z-DSs displayed a thickness of 3.9 nm as determined by atomic force microscopy and cryo-TEM irrespective of the formation method (**Figure 2**a,b, Figures S21 and S22, Supporting Information). This thickness closely resembles the ones of liposomes and cell membranes (≈4 nm).[22] We assessed the flexibility by analyzing the membrane bending rigidity through fluctuation spectroscopy.[6b,23] For comparative studies we prepared liposomes from DLPC and the more commonly utilized POPC phospholipid having membrane thicknesses of 3.1 and 3.7 nm, respectively.[24] We chose DLPC due to a similar hydrophobic chain length compared to JD^{PC} (C12). POPC contains one saturated C16 chain and a C18 chain bearing one double bond. First, we assessed the angular fluctuation of radii of deflated vesicles as a qualitative observation of their flexibility. The thermal energy was sufficient to cause fluctuations across the whole membrane, which were close to the ones observed in liposomes as depicted in the angular distribution of radii (Figure S24, Supporting Information). On the other hand, polymersomes assembled from block copolymers of poly(BD_{87}-*b*-EO_{72}) displayed hardly any fluctuation at room temperature (Figure S24, Supporting Information). These qualitative observations are subjected to the degree of deflation of the specific vesicles investigated. To quantitatively characterize the bending modulus (κ), which measures the resistance of the membrane to bend, we investigated the fluctuation spectra of giant vesicles using contour detection and Fourier analysis.[23a,c,25] Remarkably, κ for z-DSs were only 20 k_BT, which is ≈15% and 65% lower than those of liposomes from DLPC and POPC, respectively. Such values indicate that z-DS membranes are highly flexible and can thereby support complex processes that require sculpturing of the membrane (Figure 2c). Similarly, the areal expansion coefficient (K_A), which measures the resistance of the membrane to stretch, was 149 mN m^{-1}, close to the one of POPC, 141 mN m^{-1} (Figure S23, Supporting Information).

We estimated the lateral mobility of the membranes by measuring the diffusion coefficient (D) of a fluorescently labeled lipid (Liss Rhod-PE) by fluorescence recovery after photobleaching of supported bilayers. z-DS membranes displayed a D of 2.4 $\mu m^2 \cdot s^{-1}$, which is in the same range as the ones for the studied liposomes (Figure 2d) and 10 to 1000 times larger than those for some polymersomes.[26] The high D of z-DSs suggests that membrane components can rapidly spatially rearrange as in cell membranes.

Another key property of living cells is the ability to reseal their membrane in events of damage. In case the membrane is punctured, the amphiphiles are required to rapidly rearrange at the edges. The energy penalty for this rearrangement is reflected in the edge tension which drives pore-closing. The larger the edge tension, the faster the pore will close.[27] We investigated the pore closure dynamics of z-DSs with the electroporation technique (Figure 2e,f and Figure S25, Supporting Information).[28] Vesicles encapsulating a solution with differing conductivity compared to the outside medium were subjected to an electric pulse. The application of the field generates a transmembrane potential and a force normal to the membrane which opens a pore. From the dynamics of the closure of the pore, we determined the edge tension of liposome and z-DS membranes using a previously reported approach.[29] The pores generated in z-DSs closed significantly faster which is reflected in a higher edge tension of 61 pN compared to DLPC and POPC for which we obtained values of 13 and 39 pN, respectively. The higher drive for pore-closure in z-DSs might be the result of reduced interdigitation or π–π interaction at the highly curved pore interface.

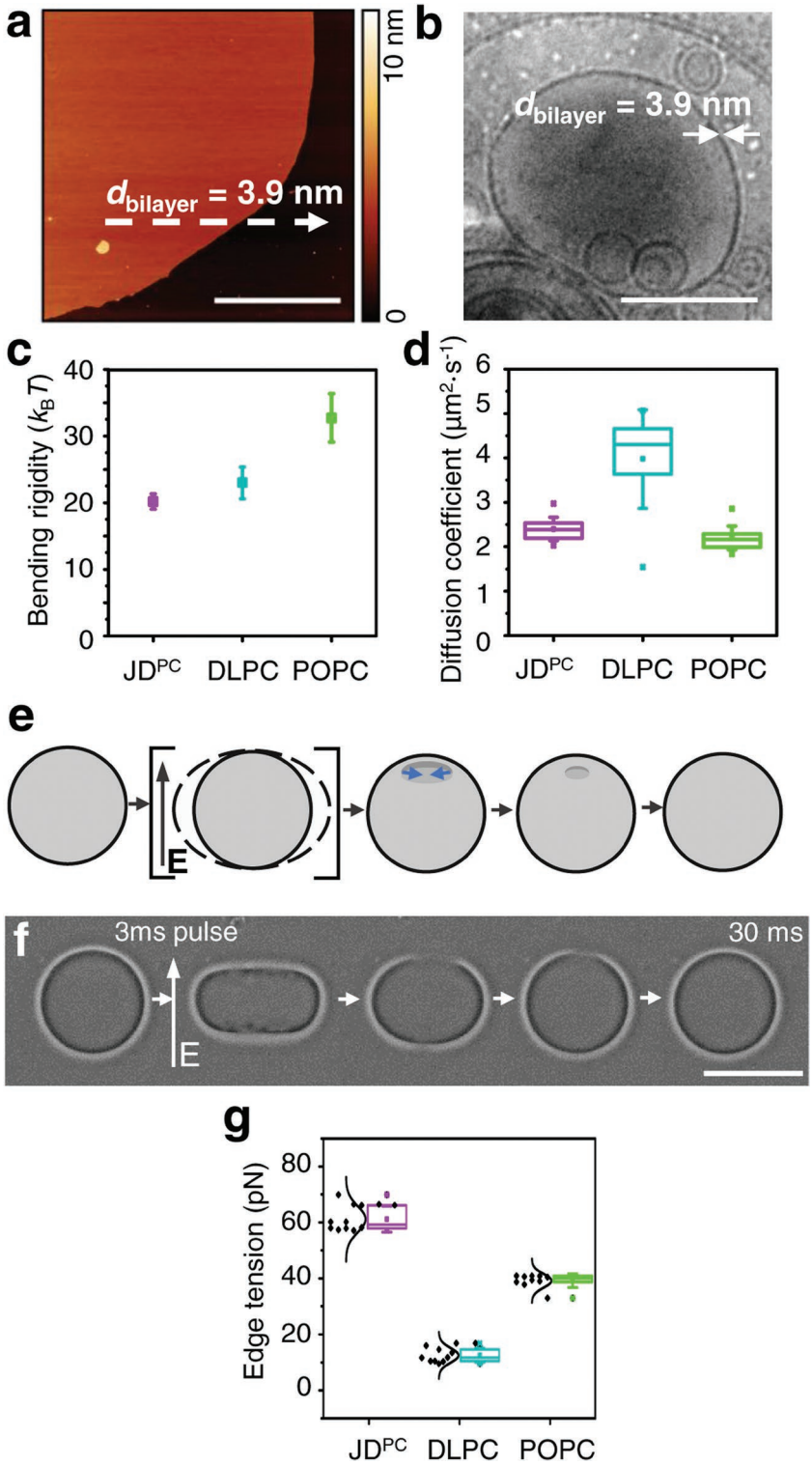

Figure 2. Physical characterization of z-DSs and comparison with DLPC and POPC liposomes. a) AFM height image of a deposited z-DS on mica. Height analysis along the white arrow yields a bilayer thickness of 3.9 nm. Scale bar: 4 μm. b) Cryo-TEM of a z-DS formed by the injection method. Contour analysis confirms the bilayer thickness of 3.9 nm. Scale bar: 200 nm. c) Bending rigidity determined by fluctuation analysis. Each point depicts the average value of six analyzed vesicles with the standard deviation. d) Diffusion coefficient calculated from fluorescence recovery after photobleaching (FRAP). e) Scheme of a vesicle undergoing electroporation. An electric field is applied for 3 ms which deforms the vesicles and creates a pore. f) Phase contrast images of the process of electroporation of z-DS showing deformation, pore formation (observed by the interrupted vesicle halo), and pore closing within 30 ms. Scale bar: 50 μm. g) Box plot and distribution of the edge tension. d,g) Each box of the boxplot was obtained from measurements on ten individual vesicles (25th–75th percentile of each data set). The median is a line and the average value is an open rectangle. The standard deviation is indicated by the whiskers while the outliers are displayed outside of the whiskers.

2.3. Stability of z-DSs

First, we examined the bench stability of JD^{PC} and z-DSs after prolonged storage under lab conditions. Neither NMR nor analytical high performance liquid chromatography showed any difference in JD^{PC} composition after 9 months of storage (Figure S14a–c, Supporting Information). Furthermore, no changes in the hydrodynamic diameter nor its distribution could be observed by dynamic light scattering of z-DSs after 3 months (Figure S14d, Supporting Information). Giant z-DSs prepared in 10×10^{-3} M HEPES buffer (pH 7.4) by thin-film hydration remained intact after 18 months storage under lab conditions (Figure S15, Supporting Information). Remarkably, giant z-DSs encapsulating calcein retained their cargo despite storage for 12 months (Figure S16, Supporting Information). In a similar vein, z-DSs displayed a higher thermal stability than its liposomal counterparts (**Figure 3**b). Giant liposomes (POPC and DLPC) and z-DSs with encapsulated green fluorescent calcein were observed in CLSM before and after heating to 80 °C for 1 h. While z-DSs remained intact (Figure 3b), liposomes formed from DLPC or POPC underwent breakage and aggregation which led to quenching of the calcein by Co^{2+} ions from

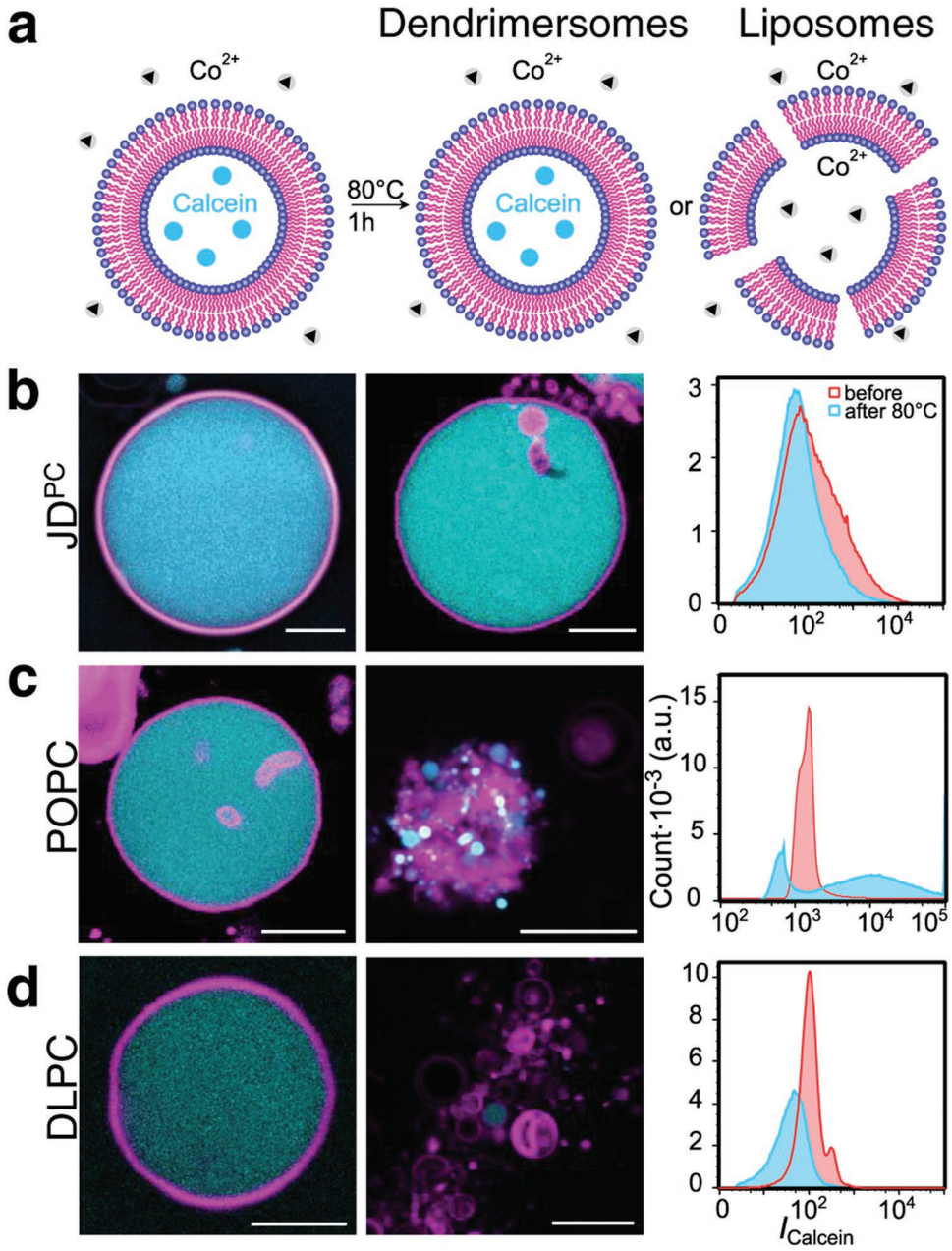

Figure 3. a) Scheme of the the experimental conditions for the analysis of the thermal stability of z-DSs and liposomes. The vesicles were formed in a calcein solution and the external calcein was quenched by the addition of Co^{2+}. b–d) Calcein-filled vesicles were heated for 1 h at 80 °C and cooled down before analysis by CLSM and FACS: b) z-DS, c,d) liposomes from POPC and DLPC, respectively. Scale bars: 10 µm.

the outer solution (Figure 3c,d). These observations were confirmed by fluorescence-activated cell sorting (FACS) before and after heating. FACS allows to investigate a much larger population of vesicles in the sample compared to CLSM. We observed no significant shift in the histogram of green fluorescence before and after heating of z-DSs confirming that the vesicles remained intact demonstrating an excellent thermal stability. Conversely, the histograms of both liposomes indicated a high degree of degradation and possible aggregation in agreement with CLSM. The overall, higher thermal and chemical stability are well in line with the higher mechanical stability as determined by puncture AFM.[30]

The higher stability of z-DSs compared to liposomes is likely related to additional cohesive interactions stemming either from the hydrophobic dendrons or the highly hydrated zwitterionic PC. To elucidate the contributors to the enhanced stability of z-DSs we compared its resistance to high temperature with other classic dendrimersomes. We formed calcein-filled dendrimersomes from JDs having non-zwitterionic triethyleneglycol-substituted benzoates hydrophilic groups while having the same single–single (JD^{s-s}) or a double (twin–twin, JD^{tw-tw}) hydrophobic dendron. The thermal treatment at 80 °C for 1 h destabilized the JD^{s-s} dendrimersomes, which now formed aggregates and drops (Figure S18, Supporting Information). On the other hand, the lumen of JD^{tw-tw} dendrimersomes remained green fluorescent, indicating that they were stable. The comparable higher stability arises from the increased hydrophobic effect stemming from the presence of two hydrophobic dendrons in JD^{tw-tw}. z-DSs displayed a high stability, comparable to those of $JD^{tw\text{-}tw}$ dendrimersomes despite being assembled from a single-single type dendrimer. This suggests that not only the hydrophobic didodecyl-substituted benzoates play a role in the enhanced stability but that additional cohesive interactions stemming from its PC group are at play.

Additionally, we examined the stability of calcein filled z-DSs under shear stress in a flow cell. They retained their cargo and remained intact even under shear stresses between τ_W = 1.47–2.45 Pa, which are comparable to values of shear stresses in physiological conditions (Figure S17, Supporting Information).

2.4. Co-Assembly Studies

We assessed the ability of JD^{PC} to form hybrid membranes with lipids by co-assembly with a fluorescently labeled 16:0 Liss Rhod-PE lipid in a lipid concentration range of 0.1–20 mol%. All lipid compositions yielded hybrid vesicles (**Figure 4**a, Figure S26, Supporting Information) without any observable phase separation in CLSM. We also examined the co-assembly with the glycolipid 16:0–18:1 DG glucose lipid (10 mol%), resulting in the preferential formation of onion-like hybrid vesicles (Figure 4b). The tendency to form onion structures is likely a result of attractive glycan–glycan interactions between glucose groups leading to a close association of the bilayers, similar to previously reported glycodendrimersomes.[31] We further studied the generation of raft-like microdomains by the co-assembly with lipids of varying saturated chain lengths between C12 and C18. Increasing the chain length increases the thermodynamic drive to generate more order phases. The polarity-sensitive fluorescent probe Laurdan is commonly utilized to visualize domains with different degrees of ordering in hybrid vesicles via generalized polarization (GP) imaging.[32] GP values range between –1 and +1 where more positive values are obtained in more ordered domains. By mapping the GP values for each pixel of hybrid vesicle images (Figure 4c) we obtained the respective GP distributions (Figure 4d). The co-assembly with DLPC (C12) and DPPC (C16) resulted in homogeneous membranes with monomodal GP distributions indicating homogeneous mixing between JD^{PC} and the lipids with no observable phase-separation. This is especially noteworthy in the case of DPPC hybrid vesicles, where the lipid's main phase transition temperature is significantly above room temperature. However, in hybrid vesicles of JD^{PC} and DSPC (C18), the larger hydrophobic mismatch drove phase separation (Figure 4d). Distinct microphases were visible in CLSM which are reflected in the GP distributions where two peaks at GP = –0.4 and GP = 0.2 stemming from the low and high ordered domains, as confirmed by analyzing each of the regions (Figure S27, Supporting Information). Interestingly, the majority of these hybrid vesicles were faceted where the flat faces are dominantly formed by more ordered green patches and curved regions between facets by less ordered blue patches stemming from DSPC-rich and JD^{PC}-rich domains (Figure 4c,d, Figures S27 and S28, Supporting Information). Phase separation in binary liposomes of DLPC with DSPC and even DAPC (C20) has been reported, but to our knowledge, none of these systems displayed faceted vesicle.[33] Such a unique behavior may be explained by a more complete segregation between DSPC and JD^{PC} enabling the crystallization of the long alkyl chains and the formation of facets.

Moreover, we studied the ability of z-DSs to integrate externally added pore-forming peptides. The addition of α-hemolysin to a suspension of calcein-filled z-DS resulted in rapid quenching of the fluorescence by Co^{2+} present in the external solution (Figure 4e). These results were confirmed by FACS where the peak position of green calcein fluorescence significantly shifted to lower intensities upon α-hemolysin addition suggesting successful formation of a pore and the transport of Co^{2+} ions into the vesicle lumen from the outer solution. The second peak, overlapping with the vesicle population before pore formation, is most likely related to multilayered vesicles where the calcein fluorescence is only quenched in between the outermost layers. The rapid formation of a functional pore without compromising the integrity of the z-DS indicates that α-hemolysin could insert, match the membrane dimensions, diffuse, and form the heptameric pore that enabled the transport of ions across an otherwise Co^{2+}-impermeable membrane. These results highlight the excellent biomimicry of z-DSs.

2.5. Interaction with Biological Media

To test the biocompatibility of z-DSs, we first studied interactions between proteins and z-DSs by observing the change of the hydrodynamic diameter of small z-DS in DLS (Figures S29b and S31, Supporting Information). z-DSs were mixed with bovine serum albumin (BSA) and lysozyme in buffer as models of anionic and cationic proteins, as well as with human blood

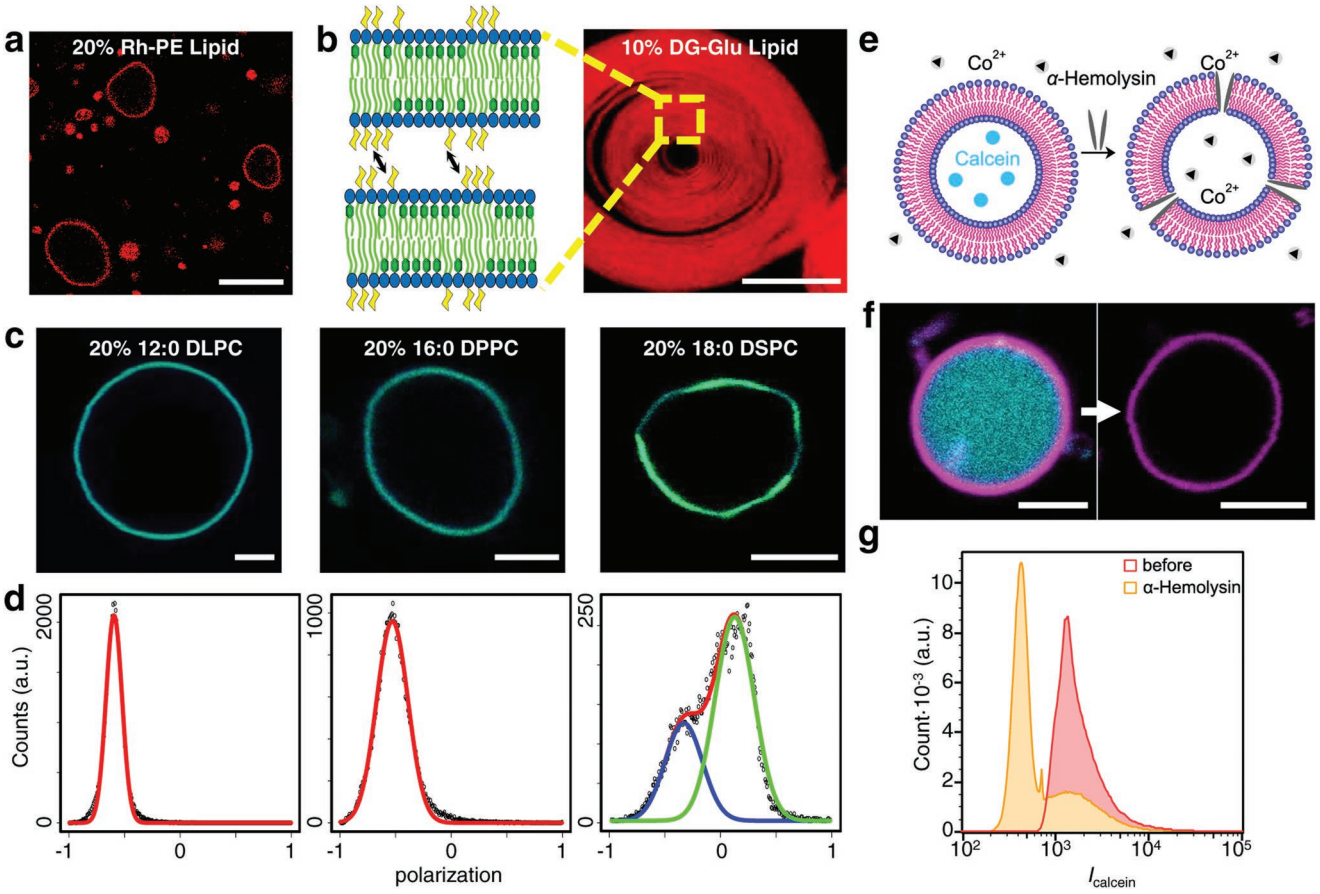

Figure 4. Co-assembly of z-DSs with structure-directing lipids and pore-forming peptides. a) Hybrid z-DS–lipid with 20 mol% of Liss Rhod-PE (red). Scale bar: 10 µm. b) Co-assembly with 10 mol% DG-Glu lipid leads to the formation of onion vesicles resulting from glycan–glycan interactions between the bilayers. c) Co-assembly of JD^{PC} with 20 mol% of lipids with varying hydrophobic chain length: DLPC (C12), DPPC (C16), and DSPC (C18). Vesicles were labeled with Laurdan as a polarity sensitive probe while the emission was detected at $\lambda_1 = 415–445$ nm (green) and $\lambda_2 = 490–530$ nm (blue). CLSM images show the merged image of both emission ranges. Scale bars: 5 µm. d) Distribution of the GP of Laurdan in z-DSs–lipid hybrids. e) Scheme of the pore formation with addition of α-hemolysin which enabled the transport and quenching of calcein fluorescence by Co^{2+}. f) CLSM images of the addition of α-hemolysin to calcein-filled z-DSs. The membrane of z-DSs was labeled with Nile red (magenta) while the vesicle lumen contains calcein (cyan). Scale bars: 5 µm. g) FACS shows a decrease in calcein fluorescence intensity after addition of α-hemolysin confirming pore formation and quenching of calcein in the lumen by Co^{2+}.

plasma (10%). Plasma is the most challenging biological fluid.[34] In all cases, we observed no increase in the hydrodynamic diameter compared to the pure vesicle dispersion, even after a contact time of 24 h. Since no detectable increase in the hydrodynamic radius occurred due to protein adsorption or vesicle aggregation, we conclude no significant fouling of the vesicles. This evaluation was also carried out for giant z-DS using CLSM. z-DSs assembled in 10×10^{-3} M HEPES buffer remained intact in BSA, lysozyme, and 10% blood plasma solutions (Figure S32, Supporting Information). Although such z-DSs were stable even in blood plasma, we observed a lower density of vesicles, presumably due to the high osmotic difference between the HEPES buffer and the blood plasma. To minimize osmotic shock, we repeated the study but formed z-DSs in sucrose solution (300×10^{-3} M) with higher osmolarity. In this case, we observed a high density of intact vesicles after an incubation time of $t = 30$ min (Figure S33, Supporting Information) and $t = 24$ h (Figure S34, Supporting Information), even in pure blood plasma. To closely monitor the interactions of proteins and giant z-DSs, we incubated vesicles with fluorescently labeled BSA (Texas Red, red) in CLSM (Figure S35, Supporting Information). After 24 h we did not observe any increase in red fluorescence signal at the membrane revealing that no significant amounts of BSA proteins had attached to the JD^{PC} membrane. Contrarily, a significant increase in red fluorescence was detected at the outer membrane periphery in the positive control which consisted of positively charged dendrimersomes co-assembled from JD^{PC}:JD^{cat} (8:2 molar ratio).

To test the compatibility with living cells, we performed a standardized colorimetric cell viability assay using three different cell types: immortalized human cancer cells (Caco-2 and HeLa), as well as cells related to human lung epithelium (H441). In all cell types, we observed a cell viability of 100% when contacted with z-DSs (Figure S29a, Supporting Information) demonstrating that z-DSs are non-cytotoxic and biocompatible. The z-DSs display an excellent biocompatibility as they maintain their structural integrity when contacted with proteins and display no cytotoxicity. Moreover, we tested whether the giant

z-DSs could be internalized into cells by incubation of fluorescently labeled z-DSs with normal human dermal fibroblasts for 24 h (Figure S30, Supporting Information). Observation by dual fluorescence/phase contrast microscopy revealed the presence of both, vesicles and fibroblasts upon mixing. After a subsequent washing step, only living fibroblasts remained, demonstrating that giant z-DSs do not attach to or internalize into cells.

2.6. Fusion with Liposomes

Vesicle fusion is an essential mechanism that drives biological processes such as intra- and inter-cellular transport, communication, signaling, protein sorting, endocytosis, and even infections.[35] To mimic the fusion process on a basic level we studied the charge-mediated fusion, which was shown to be very efficient for liposomes.[36] Here, we investigated charge-mediated fusion of JD^{PC} vesicles with liposomes by CLSM as giant vesicles. Cationic DSs were prepared by co-assembling JD^{PC} with JD^{cat} and labeling with red-fluorescent Liss Rhod-PE. Anionic liposomes were prepared by the co-assembly of DLPC with DLPG and labeled with green-fluorescent NBD-PC lipid (**Figure 5**, Figures S36 and S38, Supporting Information). Upon mixing the two vesicle dispersions, we observed three dominant behaviors (Figure 5): 1) vesicles with one fluorescence signal indicating no fusion, 2) adhesion between z-DSs and liposomes visualized by the distinctly different fluorescence of the systems, and 3) vesicles with an overlap of both fluorescence signals across the whole membrane demonstrating full fusion. To estimate fusion efficiency, we analyzed CLSM images of 410 vesicles after 4 h of incubation (Figure S39, Supporting Information). Based on the ratio of remaining unfused vesicles we estimate that 92% of possible fusion events occurred. Additionally, we studied global behavior by fluorescence resonance energy transfer (FRET) using fluorescence spectroscopy (Figure 5c).[37] Acceptor vesicles were assembled from DLPC:DLPG (8:2 molar ratio) containing no dye. Donor vesicles were assembled from JD^{PC}:JD^{cat} (8:2 molar ratio) containing two FRET dyes (0.5 mol% Liss Rhod-PE and 0.5 mol% NBD-PE). The close proximity of the fluorescent dyes in the donor vesicles results in their quenching. Fusion between donor and acceptor vesicles increases the fluorescence intensity as the dyes are diluted over the additional membrane area and thereby their respective distance increases. The maximum fluorescence intensity was obtained by adding Triton X to the donor DSs (Figure S37, Supporting Information).[13d] Obtained fluorescence intensities were calculated relative to the determined maximum. Upon addition of acceptor vesicles to the donor dendrimersomes at t = 200 s, we observed an increase in the relative fluorescence intensity which reached a plateau of 40% after 2500 s. These results demonstrate successful fusion and incorporation of both dyes inside the generated JD–lipid hybrid vesicles. Cationic DSs also underwent fusion with neutral liposomes indicating favorable kinetics, despite a lack of opposing charges (Figure S40, Supporting Information). Since no fusion occurred when neutral z-DSs were mixed with neutral or anionic liposomes (Figure S41, Supporting Information), we hypothesize that the conical shape of JD^{cat} stabilizes the energetically unfavorable inverted micellar intermediate during fusion and thereby reducing the imposed kinetic barrier.[38] However, the lack of opposing charges led to a decreased efficiency as only an estimated 37% of possible fusion events occurred within 4 h.

We additionally studied the fusion of small vesicles (D_h < 140 nm) by DLS (Figure S42, Supporting Information). Hybrid vesicles of fused cationic DSs and anionic liposomes displayed sizes that are consistent with theoretical values for binary fusion assuming conservation of volume (Section 4.16.4, Supporting Information). Other vesicle compositions did not afford vesicles with a measurable increase in size due to less efficiency or overall lack of fusion.

2.7. Motility

Living organisms heavily depend on cell motility for survival, feeding, and mass transport. Their locomotion requires significant amounts of energy since cells operate at low Reynolds numbers where they experience viscous forces that dominate the inertial ones.[39] As a result, cells have evolved various mechanisms for cell motility that rely on complex machinery. However, much simpler propulsion methods based on enzymatic decomposition of small molecules accompanied by gas formation have been utilized in liposomes and polymersomes.[40] H_2O_2 is often used as a chemical fuel that can be readily transported inside the lumen to enzymatically decompose into innocuous water and oxygen by catalase to provide propulsion.[41] We used a minimal system to harvest chemical energy from externally supplied H_2O_2 to enable propulsion. We encapsulated catalase in the lumen of z-DSs. No motion was observed in the absence of H_2O_2 as shown in **Figure 6**a and Figure S26, Supporting Information. Addition of H_2O_2 and mixing followed by observation in a chamber (10 min after addition) resulted in significant movement of vesicles across the medium (Figure 6b). Initially, (less than 15 min) the motion appears random while later there seems to be a correlated motion. To rule out convection as a possible artifact we examined the mean square displacement (MSD, Figure S43, Supporting Information) which showed no parabolic component demonstrating the motion was not convective. Moreover, the MSD followed a linear function in the first 15 min and in the last 8 min indicating diffusive motion on average well in line with propulsion after fuel consumption. The broken segments in between indicate the driven motion in random directions.[42]

2.8. z-DSs Sense the Presence of H_2O_2 in Their Surrounding

Cells use chemistry as a language to communicate with each other.[43] They produce and release signaling molecules to elicit responses by neighboring cells. An example of such molecules is H_2O_2. Elevated hydrogen peroxide levels are expressed by cells under oxidative stress or in cancer cells. Neighboring cells sense H_2O_2 and respond by initiating processes related to preventing and repairing oxidative damage.[44] Building artificial cells that are able to sense biomolecules is regarded as a key technology to bridge the gap between synthetic and natural

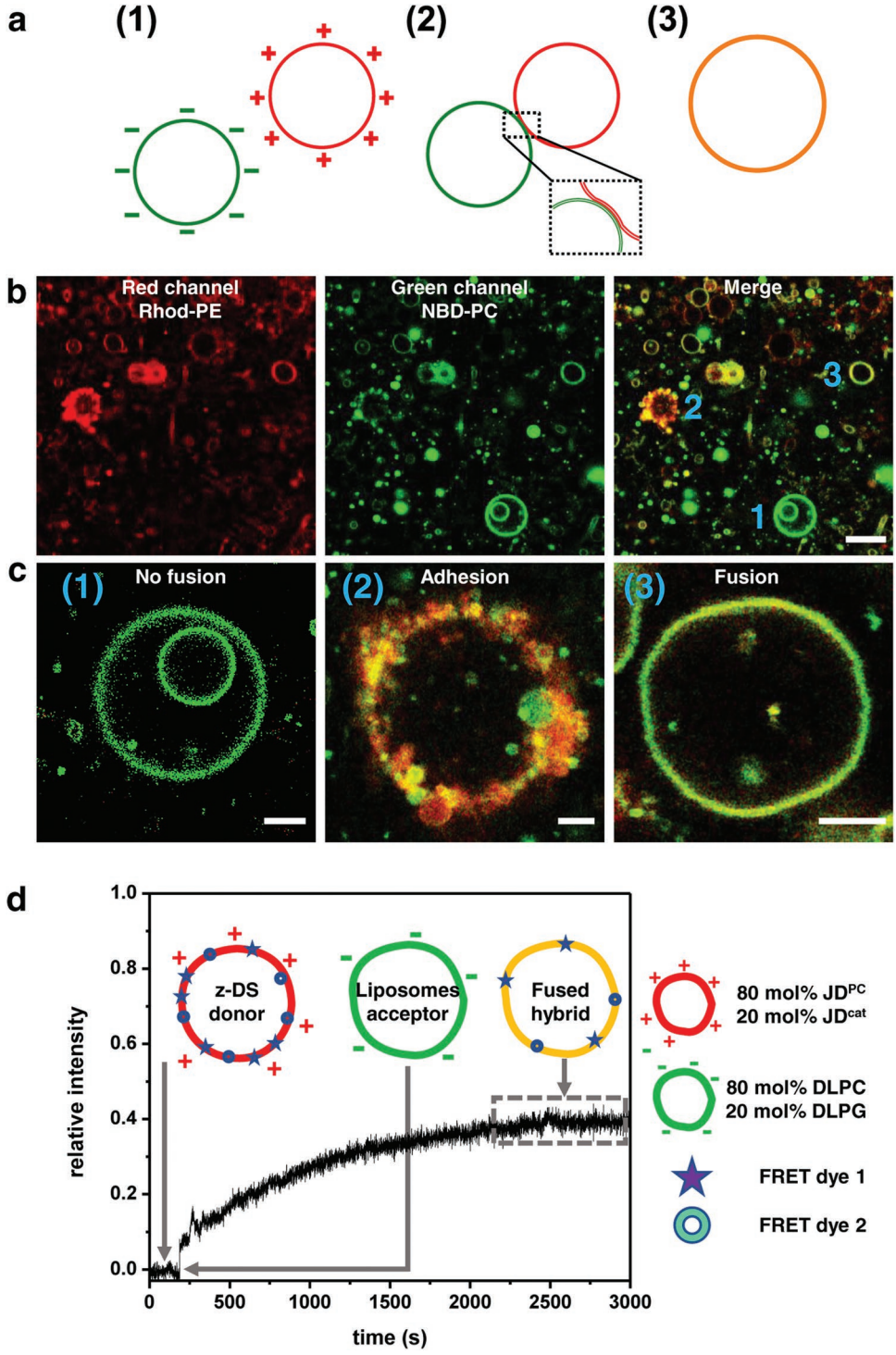

Figure 5. Fusion of DSs with liposomes driven by electrostatic interactions. a) Scheme of the fusion process: 1) The negatively charged liposomes (green) are attracted to a positively charged DSs (red) due to Coulombic interactions. 2) This is followed by adhesion and docking with the concomitant bending of the contact region. 3) Fusion proceeds few minutes afterward and the dyes are exchanged which yields an apparent orange color in the merged CLSM image. b) CLSM overview after mixing of positively charged JD^{PC}:JD^{cat} (8:2 molar ratio) DSs (1 mol% Liss Rhod-PE, red) and negatively charged DLPC:DLPG (8:2 molar ratio) liposomes (1 mol% NBD-PC, green). c) Selected vesicles showing: 1) no fusion, 2) adhesion, or 3) full fusion. d) A large population of vesicles was studied by FRET using fluorescence spectroscopy where the donor contains both FRET dyes. Upon addition of acceptor vesicles, a fluorescence increase was detected consistent with the formation of fused hybrids. Scale bars: 20 µm in (a) and 5 µm in (b).

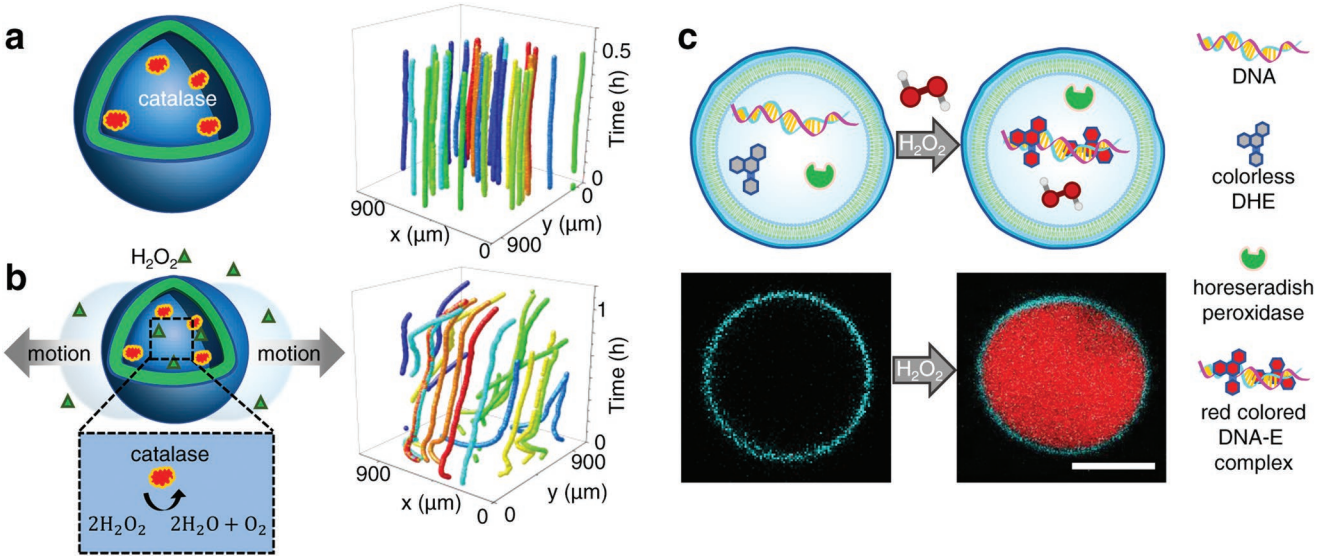

Figure 6. Programming motility in z-DSs. a) The position of catalase-filled z-DSs was monitored in CLSM for 30 min. Within the observation time the position of the vesicles in *x* and *y* remained constant. b) In contrast, after addition of hydrogen peroxide, the vesicles exhibited strong motion. The movement is due to catalase that catalyzes a reaction within the vesicle lumen leading to a decomposition of hydrogen peroxide into water and oxygen. c) z-DSs are utilized as a biosensor. Within z-DSs we encapsulated DNA, horseradish peroxidase (HRP), and dihydroethidium (DHE). Upon addition of membrane permeable hydrogen peroxide in the external solution, a red colored DNA-E complex is formed within the vesicle lumen. The generation of red fluorescence within the lumen was monitored by CLSM. The membrane was labeled with 1 mol% Laurdan. Scale bar: 5 µm.

cells. We formed H_2O_2-detecting z-DSs by encapsulating horseradish peroxidase and DNA and incubating them with membrane-permeable dihydroethidium (DHE) (Figure 6c). Upon addition of H_2O_2, HRP catalyzed the oxidation of DHE to ethidium (E) which intercalates with DNA to generate a red fluorescent product within the z-DS lumen.[45]

We performed control experiments that exclude any effect of the laser that was used for excitation of the dye and proved that only upon addition of H_2O_2 fluorescence within the vesicle lumen was generated (Figure S44, Supporting Information). We utilized fluorescence spectroscopy as a more sensitive technique to study the global behavior z-DSs that were prepared in the same manner. The addition of H_2O_2 led to an immediate gradual increase in fluorescence intensity that reached a plateau after 2000 s. Under these conditions a H_2O_2 concentration as low as 35 µM was detectable (Figure S45, Supporting Information). These results demonstrate the first steps toward the production of synthetic biosensors to detect environments with elevated H_2O_2 concentrations in medical applications or environmental science.

3. Conclusion

We have introduced a new concept for cell-membrane mimicry based on the self-assembly of a JD bearing a PC headgroup (JD^{PC}) into z-DSs. In the molecular design of JD^{PC} we strategically eliminated the weak points that cause degradation and low stability of liposomes. This resulted in membranes with a higher chemical and mechanical stability compared to liposomes. The resulting vesicles mimic the periphery of natural cell membranes, as well as their most essential physical properties such as bilayer thickness, flexibility, and lateral mobility. Such high level of biomimicry enabled the incorporation of lipids, glycolipids, and protein pores. Functionalization of the membrane with structure directing lipids allowed us to program the formation of onion-type vesicles and raft-like domains. We employed these z-DSs to mimic essential cellular functions such as fusion, environmental sensing, and motility on a basic level. We envision that our system offers a platform for minimal cell mimics that, despite their synthetic nature, can integrate and interact with living matter. It offers a superior alternative to liposomes by virtue of its chemical stability that not only improves handling and usage in mild conditions but also allows studies at elevated temperatures.

4. Experimental Section

Statistical Analysis: The reported syntheses were performed at least twice to confirm the reproducibility of the results. All directly measured data were presented without pre-processing unless stated otherwise. All boxplots were generated from at least 10 data points containing 25–75% of the data set. Qualitative angular fluctuation analysis in Figure S24, Supporting Information was performed on a single snapshot of a representative vesicle for each composition while quantitative analysis of bending rigidities is depicted in the interval plots in Figure 2c which were generated from 6 data points for each composition. Protein experiments were performed in triplicate. For temperature stability, insertion of α-hemolysin, biocompatibility in protein solutions and blood plasma, sensing, as well as fusion we obtained data on different locations by always studying a population of giant and small vesicles, respectively. For CLSM we show multiple CLSM overviews and selected representative single vesicles. Additional quantitative characterization was done in FACS with 15 000 events per sample, in FRET using fluorescence spectroscopy and in DLS. The analysis of vesicle size distribution was performed with 100 vesicles (Figure S20, Supporting Information) while for the calculation of fusion efficiency 410 and 344 vesicles were analyzed from CLSM images (Table S6, Supporting

Information). The interval plots in Figure S23a, Supporting Information were generated from 13 data points for z-DSs and 6 for POPC liposomes. All data were processed according to the description in the respective supporting information section. Statistical analysis and data fitting were performed in OriginPro2018, Python, and R.

Supporting Information

Supporting Information is available from the Wiley Online Library or from the author.

Acknowledgements

This project was financially supported by the European Commission within a H2020-NMBP-TR-IND-2018, EVPRO grant 814495-2. Moreover, the authors acknowledge support of RWTH University via the calls Innovation Sprint 2021 (project ANVIVES) as part of the "Exzellenz Start-up Center NRW" initiative and ERS Seed Fund Project SFSynt003 and ERS Seed Fund Project SFSynt005. IBEC is a member of the CERCA program. M.A. acknowledges funding from International Max Planck Research School on Multiscale Bio-Systems (IMPRS).

Open access funding enabled and organized by Projekt DEAL.

Conflict of Interest

The authors declare no conflict of interest.

Data Availability Statement

The data that support the findings of this study are available from the corresponding author upon reasonable request.

Keywords

biosensors, bottom-up synthetic biology, hybrid vesicles, synthetic cells, vesicle fusion, vesicle motility, zwitterionic dendrimersomes

Received: July 11, 2022
Revised: September 7, 2022
Published online:

[1] a) P. Schwille, *Science* **2011**, *333*, 1252; b) P. Schwille, J. Spatz, K. Landfester, E. Bodenschatz, S. Herminghaus, V. Sourjik, T. J. Erb, P. Bastiaens, R. Lipowsky, A. Hyman, P. Dabrock, J.-C. Baret, T. Vidakovic-Koch, P. Bieling, R. Dimova, H. Mutschler, T. Robinson, T. Y. D. Tang, S. Wegner, K. Sundmacher, *Angew. Chem., Int. Ed.* **2018**, *57*, 13382; c) R. J. Brea, M. D. Hardy, N. K. Devaraj, *Chem. - Eur. J.* **2015**, *21*, 12564; d) F. Lussier, O. Staufer, I. Platzman, J. P. Spatz, *Trends Biotechnol.* **2021**, *39*, 445.

[2] a) S. J. Singer, G. L. Nicolson, *Science* **1972**, *175*, 720; b) H. F. Lodish, *Molecular Cell Biology*, W. H. Freeman, New York **2016**.

[3] a) F. Bezanilla, *Nat. Rev. Mol. Cell Biol.* **2008**, *9*, 323; b) K. Keren, *Eur. Biophys. J.* **2011**, *40*, 1013; c) D. C. Gadsby, *Nat. Rev. Mol. Cell Biol.* **2009**, *10*, 344.

[4] O. G. Mouritsen, M. Bloom, *Biophys. J.* **1984**, *46*, 141.

[5] D. Morzy, M. Bastings, *Angew. Chem., Int. Ed.* **2022**, *61*, e202114167.

[6] a) W. Rawicz, K. C. Olbrich, T. McIntosh, D. Needham, E. Evans, *Biophys. J.* **2000**, *79*, 328; b) R. Dimova, *Adv. Colloid Interface Sci.* **2014**, *208*, 225.

[7] M. Grit, D. J. A. Crommelin, *Chem. Phys. Lipids* **1993**, *64*, 3.

[8] a) A. Reis, C. M. Spickett, *Biochim. Biophys. Acta, Biomembr.* **2012**, *1818*, 2374; b) E. Schnitzer, I. Pinchuk, D. Lichtenberg, *Eur. Biophys. J.* **2007**, *36*, 499; c) K. A. Runas, N. Malmstadt, *Soft Matter* **2015**, *11*, 499.

[9] B. M. Discher, Y. Y. Won, D. S. Ege, J. C. Lee, F. S. Bates, D. E. Discher, D. A. Hammer, *Science* **1999**, *284*, 1143.

[10] a) J. Lefley, C. Waldron, C. R. Becer, *Polym. Chem.* **2020**, *11*, 7124; b) M. Massignani, H. Lomas, G. Battaglia, in *Modern Techniques for Nano- and Microreactors/-reactions*, Advances in Polymer Science, Vol. *229* (Ed: F. Caruso), Springer, Berlin/Heidelberg, Germany **2010**, Ch. 40; c) E. Rideau, R. Dimova, P. Schwille, F. R. Wurm, K. Landfester, *Chem. Soc. Rev.* **2018**, *47*, 8572.

[11] a) H. Bermúdez, D. A. Hammer, D. E. Discher, *Langmuir* **2004**, *20*, 540; b) R. Dimova, U. Seifert, B. Pouligny, S. Förster, H. G. Döbereiner, *Eur. Phys. J. E: Soft Matter Biol. Phys.* **2002**, *7*, 241.

[12] a) F. Itel, M. Chami, A. Najer, S. Lörcher, D. Wu, I. A. Dinu, W. Meier, *Macromolecules* **2014**, *47*, 7588; b) A. Mecke, C. Dittrich, W. Meier, *Soft Matter* **2006**, *2*, 751; c) F. Itel, A. Najer, C. G. Palivan, W. Meier, *Nano Lett.* **2015**, *15*, 3871; d) G. Srinivas, D. E. Discher, M. L. Klein, *Nano Lett.* **2005**, *5*, 2343.

[13] a) L. Otrin, A. Witkowska, N. Marušič, Z. Zhao, R. B. Lira, F. L. Kyrilis, F. Hamdi, I. Ivanov, R. Lipowsky, P. L. Kastritis, R. Dimova, K. Sundmacher, R. Jahn, T. Vidaković-Koch, *Nat. Commun.* **2021**, *12*, 4972; b) N. Marušič, L. Otrin, Z. Zhao, R. B. Lira, F. L. Kyrilis, F. Hamdi, P. L. Kastritis, T. Vidaković-Koch, I. Ivanov, K. Sundmacher, R. Dimova, *Proc. Natl. Acad. Sci. USA* **2020**, *117*, 15006; c) M. Chemin, P.-M. Brun, S. Lecommandoux, O. Sandre, J.-F. L. Meins, *Soft Matter* **2012**, *8*, 2867; d) N. Marušič, L. Otrin, J. Rauchhaus, Z. Zhao, F. L. Kyrilis, F. Hamdi, P. L. Kastritis, R. Dimova, I. Ivanov, K. Sundmacher, *Proc. Natl. Acad. Sci. USA* **2022**, *119*, e2122468119.

[14] T. P. T. Dao, A. Brûlet, F. Fernandes, M. Er-Rafik, K. Ferji, R. Schweins, J. P. Chapel, A. Fedorov, M. Schmutz, M. Prieto, O. Sandre, J. F. Le Meins, *Langmuir* **2017**, *33*, 1705.

[15] A. M. Wagner, J. Quandt, D. Söder, M. Garay-Sarmiento, A. Joseph, V. S. Petrovskii, L. Witzdam, T. Hammoor, P. Steitz, T. Haraszti, I. I. Potemkin, N. Y. Kostina, A. Herrmann, C. Rodriguez-Emmenegger, *Adv. Sci.* **2022**, *9*, 2200617.

[16] a) V. Percec, D. A. Wilson, P. Leowanawat, C. J. Wilson, A. D. Hughes, M. S. Kaucher, D. A. Hammer, D. H. Levine, A. J. Kim, F. S. Bates, K. P. Davis, T. P. Lodge, M. L. Klein, R. H. DeVane, E. Aqad, B. M. Rosen, A. O. Argintaru, M. J. Sienkowska, K. Rissanen, S. Nummelin, J. Ropponen, *Science* **2010**, *328*, 1009; b) S. E. Sherman, Q. Xiao, V. Percec, *Chem. Rev.* **2017**, *117*, 6538.

[17] a) D. Zhang, E. N. Atochina-Vasserman, D. S. Maurya, N. Huang, Q. Xiao, N. Ona, M. Liu, H. Shahnawaz, H. Ni, K. Kim, M. M. Billingsley, D. J. Pochan, M. J. Mitchell, D. Weissman, V. Percec, *J. Am. Chem. Soc.* **2021**, *143*, 12315; b) Q. Xiao, S. S. Yadavalli, S. Zhang, S. E. Sherman, E. Fiorin, L. da Silva, D. A. Wilson, D. A. Hammer, S. Andre, H. J. Gabius, M. L. Klein, M. Goulian, V. Percec, *Proc. Natl. Acad. Sci. USA* **2016**, *113*, E1134; c) S. S. Yadavalli, Q. Xiao, S. E. Sherman, W. D. Hasley, M. L. Klein, M. Goulian, V. Percec, *Proc. Natl. Acad. Sci. USA* **2019**, *116*, 744.

[18] a) N. Yu. Kostina, D. Söder, T. Haraszti, Q. Xiao, K. Rahimi, B. E. Partridge, M. L. Klein, V. Percec, C. Rodriguez-Emmenegger, *Angew. Chem., Int. Ed.* **2021**, *60*, 8352; b) C. Rodriguez-Emmenegger, Q. Xiao, N. Y. Kostina, S. E. Sherman, K. Rahimi,

B. E. Partridge, S. Li, D. Sahoo, A. M. Reveron Perez, I. Buzzacchera, H. Han, M. Kerzner, I. Malhotra, M. Moller, C. J. Wilson, M. C. Good, M. Goulian, T. Baumgart, M. L. Klein, V. Percec, *Proc. Natl. Acad. Sci. USA* **2019**, *116*, 5376; c) N. Y. Kostina, A. M. Wagner, T. Haraszti, K. Rahimi, Q. Xiao, M. L. Klein, V. Percec, C. Rodriguez-Emmenegger, *Soft Matter* **2021**, *17*, 254.

[19] S. Zhang, H.-J. Sun, A. D. Hughes, B. Draghici, J. Lejnieks, P. Leowanawat, A. Bertin, L. Otero De Leon, O. V. Kulikov, Y. Chen, D. J. Pochan, P. A. Heiney, V. Percec, *ACS Nano* **2014**, *8*, 1554.

[20] a) M. Peterca, V. Percec, P. Leowanawat, A. Bertin, *J. Am. Chem. Soc.* **2011**, *133*, 20507; b) I. Buzzacchera, Q. Xiao, H. Han, K. Rahimi, S. Li, N. Y. Kostina, B. J. Toebes, S. E. Wilner, M. Möller, C. Rodriguez-Emmenegger, T. Baumgart, D. A. Wilson, C. J. Wilson, M. L. Klein, V. Percec, *Biomacromolecules* **2019**, *20*, 712.

[21] a) R. Dimova, C. M. Marques, *The Giant Vesicle Book*, CRC Press, Boca Raton, FL, USA **2019**; b) R. Dimova, *Annu. Rev. Biophys.* **2019**, *48*, 93.

[22] K. Mitra, I. Ubarretxena-Belandia, T. Taguchi, G. Warren, D. M. Engelman, *Proc. Natl. Acad. Sci. USA* **2004**, *101*, 4083.

[23] a) R. S. Gracià, N. Bezlyepkina, R. L. Knorr, R. Lipowsky, R. Dimova, *Soft Matter* **2010**, *6*, 1472; b) H. A. Faizi, S. L. Frey, J. Steinkühler, R. Dimova, P. M. Vlahovska, *Soft Matter* **2019**, *15*, 6006; c) H. A. Faizi, C. J. Reeves, V. N. Georgiev, P. M. Vlahovska, R. Dimova, *Soft Matter* **2020**, *16*, 8996.

[24] a) N. Kučerka, Y. Liu, N. Chu, H. I. Petrache, S. Tristram-Nagle, J. F. Nagle, *Biophys. J.* **2005**, *88*, 2626; b) N. Kučerka, S. Tristram-Nagle, J. F. Nagle, *J. Membr. Biol.* **2006**, *208*, 193.

[25] J. Pécréaux, H. G. Döbereiner, J. Prost, J. F. Joanny, P. Bassereau, *Eur. Phys. J. E: Soft Matter Biol. Phys.* **2004**, *13*, 277.

[26] J. C. M. Lee, M. Santore, F. S. Bates, D. E. Discher, *Macromolecules* **2002**, *35*, 323.

[27] F. Brochard-Wyart, P. G. De Gennes, O. Sandre, *Phys. A* **2000**, *278*, 32.

[28] K. A. Riske, R. Dimova, *Biophys. J.* **2005**, *88*, 1143.

[29] a) T. Portet, R. Dimova, *Biophys. J.* **2010**, *99*, 3264; b) R. B. Lira, F. S. C. Leomil, R. J. Melo, K. A. Riske, R. Dimova, *Adv. Sci.* **2021**, *8*, 2004068; c) F. S. C. Leomil, M. Zoccoler, R. Dimova, K. A. Riske, *Bioinf. Adv.* **2021**, *1*, vbab037.

[30] A. M. Wagner, H. Eto, A. Joseph, S. Kohyama, T. Haraszti, R. A. Zamora, M. Vorobii, M. I. Giannotti, P. Schwille, C. Rodriguez-Emmenegger, *Adv. Mater.* **2022**, *34*, 2202364.

[31] Q. Xiao, S. Zhang, Z. Wang, S. E. Sherman, R.-O. Moussodia, M. Peterca, A. Muncan, D. R. Williams, D. A. Hammer, S. Vértesy, S. André, H.-J. Gabius, M. L. Klein, V. Percec, *Proc. Natl. Acad. Sci. USA* **2016**, *113*, 1162.

[32] L. A. Bagatolli, *Biochim. Biophys. Acta, Biomembr.* **2006**, *1758*, 1541.

[33] L. A. Bagatolli, E. Gratton, *Biophys. J.* **2000**, *79*, 434.

[34] a) C. Rodriguez Emmenegger, E. Brynda, T. Riedel, Z. Sedlakova, M. Houska, A. B. Alles, *Langmuir* **2009**, *25*, 6328; b) K. Ishihara, N. P. Ziats, B. P. Tierney, N. Nakabayashi, J. M. Anderson, *J. Biomed. Mater. Res.* **1991**, *25*, 1397; c) K. Ishihara, H. Nomura, T. Mihara, K. Kurita, Y. Iwasaki, N. Nakabayashi, *J. Biomed. Mater. Res.* **1998**, *39*, 323.

[35] R. Jahn, T. Lang, T. C. Südhof, *Cell* **2003**, *112*, 519.

[36] R. B. Lira, T. Robinson, R. Dimova, K. A. Riske, *Biophys. J.* **2019**, *116*, 79.

[37] R. B. Lira, R. Dimova, in *Advances in Biomembranes and Lipid Self-Assembly*, Vol. *30* (Ed: R. Lipowsky), Academic Press, San Diego, CA, USA **2019**, pp. 229–270.

[38] a) D. P. Siegel, *Biophys. J.* **1984**, *45*, 399; b) H. Ellens, D. P. Siegel, D. Alford, P. L. Yeagle, L. Boni, L. J. Lis, P. J. Quinn, J. Bentz, *Biochemistry* **1989**, *28*, 3692; c) P. R. Cullis, M. J. Hope, *Nature* **1978**, *271*, 672.

[39] E. Lauga, T. R. Powers, *Rep. Prog. Phys.* **2009**, *72*, 096601.

[40] L. Wang, S. Song, J. Hest, L. K. E. A. Abdelmohsen, X. Huang, S. Sánchez, *Small* **2020**, *16*, 1907680.

[41] T. Patiño, X. Arqué, R. Mestre, L. Palacios, S. Sánchez, *Acc. Chem. Res.* **2018**, *51*, 2662.

[42] W. S. Jang, H. J. Kim, C. Gao, D. Lee, D. A. Hammer, *Small* **2018**, *14*, 1801715.

[43] S. Mann, *Acc. Chem. Res.* **2012**, *45*, 2131.

[44] E. A. Veal, A. M. Day, B. A. Morgan, *Mol. Cell* **2007**, *26*, 1.

[45] a) N. Patsoukis, I. Papapostolou, C. D. Georgiou, *Anal. Bioanal. Chem.* **2005**, *381*, 1065; b) J. Zielonka, S. Srinivasan, M. Hardy, O. Ouari, M. Lopez, J. Vasquez-Vivar, N. G. Avadhani, B. Kalyanaraman, *Free Radical Biol. Med.* **2008**, *44*, 835.